

Article

Exploration of D0₂₂-Type Al₃TM (TM = Sc, Ti, V, Zr, Nb, Hf, Ta): Elastic Anisotropy, Electronic Structures, Work Function and Experimental Design

Guowei Zhang ^{1,*}, Fenger Sun ^{1,*}, Heping Liu ¹, Xiaoyan Ren ², Hong Xu ¹, Mingjie Wang ¹  and Yizheng Fu ¹

¹ School of Material Science and Engineering, North University of China, Taiyuan 030051, China; peace666@126.com (H.L.); xuhong@nuc.edu.cn (H.X.); 15513882577@163.com (M.W.); fuyizheng@nuc.edu.cn (Y.F.)

² Department of Mechanical Engineering, Taiyuan Institute of Technology, Taiyuan 030008, China; renxiaoyan03@126.com

* Correspondence: 20030358@nuc.edu.cn (G.Z.); peace666@nuc.edu.cn (F.S.); Tel.: +86-0351-355-7519 (G.Z.)

Abstract: The structural properties, elastic anisotropy, electronic structures and work function of D0₂₂-type Al₃TM (TM = Sc, Ti, V, Y, Zr, Nb, La, Hf, Ta) are studied using the first-principles calculations. The results indicate that the obtained formation enthalpy and cohesive energy of these compounds are in accordance with the other calculated values. It is found that the Al₃Zr is the most thermodynamic stable compound. The mechanical property indexes, such as elastic constants, bulk modulus, shear modulus, Young's modulus, Poisson's ratio, and Vickers hardness are systematically explored. Moreover, the calculated universal anisotropic index, percent anisotropy and shear anisotropic factors of D0₂₂-type Al₃TM are analyzed carefully. It demonstrates that the shear modulus anisotropy of Al₃La is the strongest, while that of Al₃Ta is the weakest. In particular, the density of states at Fermi level is not zero, suggesting that these phases have metal properties and electrical conductivity. More importantly, the mechanisms of correlation between hardness and Young's modulus are further explained by the work function. Finally, the experimental design proves that D0₂₂-Al₃Ta has an excellent strengthening effect.

Keywords: trialuminides; structural properties; mechanical anisotropy; work function; experimental design; orientation relationship



Citation: Zhang, G.; Sun, F.; Liu, H.; Ren, X.; Xu, H.; Wang, M.; Fu, Y. Exploration of D0₂₂-Type Al₃TM (TM = Sc, Ti, V, Zr, Nb, Hf, Ta): Elastic Anisotropy, Electronic Structures, Work Function and Experimental Design. *Materials* **2021**, *14*, 2206. <https://doi.org/10.3390/ma14092206>

Academic Editor: Bryan M. Wong

Received: 19 March 2021

Accepted: 21 April 2021

Published: 25 April 2021

Publisher's Note: MDPI stays neutral with regard to jurisdictional claims in published maps and institutional affiliations.



Copyright: © 2021 by the authors. Licensee MDPI, Basel, Switzerland. This article is an open access article distributed under the terms and conditions of the Creative Commons Attribution (CC BY) license (<https://creativecommons.org/licenses/by/4.0/>).

1. Introduction

With the increasing demand of aerospace and automotive industry for structural material properties, aluminum rich compounds containing transition metal (TM, i.e., Sc, Ti, V, Y, Zr, Nb, La, Hf, Ta) elements have attracted extensive attention [1–3]. Among them, trialuminides (Al₃TM) are the most potential candidate compounds, mainly because it can meet a variety of advantages, such as a high melting point, good thermal conductivity, low temperature damage resistance, strong creep resistance, and high specific strength. Furthermore, most of these intermetallics have different crystal structures of L1₂, D0₁₉, D0₂₂, or D0₂₃ [4–11]. Usually, the Al₃TM series of trialuminides can crystallize into the cubic L1₂ (space group Pm $\bar{3}$ m) and tetragonal D0₂₂ (space group I4/mmm) crystal structures. The L1₂ structure has better ductility due to its higher symmetry and more slip systems. However, it is generally believed that the lower symmetry of D0₂₂ structure is the main cause of poor ductility. Many attempts had been made to convert D0₂₂ into L1₂, which can make the aluminide have good ductility [12–15]. However, the D0₂₂ structure has a good strengthening effect in the recent design of high entropy alloy. Hereinto, one of the critical challenges is to explore the internal mechanism of D0₂₂-type trialuminides.

Previous studies have made a lot of efforts to reveal the properties of these intermetallic compounds. Recently, Jahnnatek M et al. [16] investigated the interatomic bonds and the

tensile anisotropy of $\text{Al}_3(\text{Sc}, \text{Ti}, \text{V}, \text{Cr})$ by using density-functional theory. Here, in both the $L1_2$ and $D0_{22}$ crystal structure, the main bonding character originates from the saturation of dominant d^3 ($L1_2$) and d^4 ($D0_{22}$) hybrid orbitals located on the TM atoms. In addition, the structural, electronic, and thermodynamic properties of $\text{Al}_3(\text{Ti}_x\text{V}_{1-x})$ alloy in $D0_{22}$ and $L1_2$ structures have been reported using the full-potential linearized augmented plane wave (FP-LAPW) method within the framework of the density functional theory (DFT) [17]. It can be drawn from this result that $D0_{22}$ is the relatively stable phase used in these materials, while $L1_2$ is always the metastable phase. In addition, the phase of $\text{Al}_3(\text{Ti}, \text{V})$ crystal and electronic structure in $D0_{22}$ and $L1_2$ were studied in detail, which indicates that the increase of charge density along the Al-(V, Ti) bond is a characteristic of bonding [18,19]. Meanwhile, Schwarz et al. [20] had explored the properties of trialuminides with ultra-fine microstructures. It can be concluded that the $D0_{22}$ structure has poor ductility because of low symmetry, which may be related to the insufficient number of slip systems in polycrystals. Chen Z et al. [21] had investigated the thermodynamic, elastic, and electronic properties of $D0_{22}$ -type Al_3V and Al_3Nb intermetallics under pressures using the first-principle method. Under the same pressure condition, the relative volume change of Al_3Nb is smaller than that of Al_3V , which is mainly because the bulk modulus of Al_3Nb is larger than that of Al_3V . By employing the Vienna ab initio simulation package (VASP), the relative stabilities of $L1_2$, $D0_{22}$ and $D0_{23}$ with different structures in the intermetallic compound ZrAl_3 were studied by Colinet C et al. [22]. The last theoretical calculations had shown that the structure of $D0_{22}$ is slightly more stable than that of $L1_2$. Li R et al. [23] studied the structural stability, electronic structures, and thermodynamic properties of HfAl_3 with $L1_2$, $D0_{22}$ and $D0_{23}$ different structures by the first-principle method. The calculated results revealed that the order of their structural stability can be arranged as $D0_{23} > D0_{22} > L1_2$. Furthermore, Boulechfar R et al. [24] conducted the investigation of the structural stability, electronic, and thermodynamic properties of Al_3Ta intermetallic compound by using the full-potential linearized augmented plane wave (FP-LAPW) computational approach. The conclusion is that the total energy and the total density of states at the Fermi level indicate that the stability of $D0_{22}$ structure is better than that of $D0_{23}$ and $L1_2$ structures. Li C et al. [25] calculated the properties of intermetallic compound Al_3TM (TM = Ti, Zr, Hf, Sc) and the interfacial properties of Al_3TM (TM = Ti, Zr, Hf, Sc) by the first principles. The calculated energy shows that Al_3Zr has the lowest formation enthalpies and is the easiest to form.

However, few systematic investigations have been performed regarding the mechanical anisotropy of trialuminides Al_3TM (TM, i.e., Sc, Ti, V, Y, Zr, Nb, La, Hf, Ta). Particularly, up to now, the first-principles study of work function of these trialuminides Al_3TM phases is almost blank. Accordingly, it is interesting to research the differences and similarities in elastic properties when the Al element forms a bond with those transition elements. Therefore, further attempts in this respect still need to research the properties of $D0_{22}$ -type trialuminides.

Indeed, when the properties of compounds are to be explored and cannot be measured by experimental means, theoretical simulation is a very effective method to forecast the properties of materials. Faithfully, the first principles calculation method based on the density functional theory (DFT) is a very powerful way to accurately study the physical properties of compounds [26,27]. Consequently, the structure, mechanical anisotropy, electronic properties, and work function of trialuminides Al_3TM (TM, i.e., Sc, Ti, V, Y, Zr, Nb, La, Hf, Ta) have been systematically explored by first-principles calculation method in the present work. Based on the simulation results, an experiment was designed to verify the simulation results. The research results can supply more theoretical and technological guidance on $D0_{22}$ -type trialuminides design.

2. Methods and Details

In order to more systematically study the internal mechanisms of $D0_{22}$ structure Al_3TM (TM = Sc, Ti, V, Y, Zr, Nb, La, Hf, Ta), the first-principle calculations based on

density functional theory are implemented in the CASTEP (Cambridge Serial Total Energy Package) code [28]. The generalized gradient approximation (GGA) method is applied to the exchange correlation function, and three parameterization ways, Perdew, Burke, and Ernzerhof (PBE) are adopted [29,30]. The $3s^23p^1$, $3s^23d^14s^2$, $3s^23p^63d^24s^2$, $3s^23p^63d^34s^2$, $4d^15s^2$, $4s^24p^64d^25s^2$, $4s^24p^64d^45s^1$, $5s^25p^65d^16s^2$, $5d^26s^2$ and $5d^36s^2$ electrons are explicitly considered as valence for Al, Sc, Ti, V, Y, Zr, Nb, La, Hf and Ta, respectively. In the process of optimization, the total energy of the self-consistent convergence condition is less than 1.0×10^{-5} eV/atom. The maximum displacement is 0.001 Å and the maximum force acting on each atom is 0.03 eV/Å. The maximum stress deviation is 0.05 GPa, while the SCF convergence accuracy is set to 5.0×10^{-7} eV/atom. Using plane wave basis set, the cutoff energy is 500 eV, while the total energy of this work will eventually converge to less than 1 meV. Based on the characteristics of $D0_{22}$ crystal type in this study, the k-point grid of energy integration in irreducible Brillouin region is generated by using the Monkhorst-Pack method. A $22 \times 22 \times 10$ k-point mesh for the static calculation is used for this work.

Based on the simulation results, we designed an experiment to verify the simulation results. A high entropy alloy reinforced by $D0_{22}$ -type Al_3Ta phase was designed. Several elements of Co, Cr, Fe, Ni and Ta powders with purity of 99.96% were used as designed materials (Co 21.6 ± 0.2 , Cr 19.8 ± 0.3 Fe 21.5 ± 0.2 Al 35.5 ± 0.3 Ta 1.6 ± 0.2 with atomic percentage). These nearly pure powders were first ball-ground and then pressed into shape. Finally, it is sintered in a vacuum tube furnace. To ensure uniformity, the alloy is smelted five times and then soldered at 1200 °C. At last, the X-ray diffraction (XRD) was tested at room temperature and operated at 30 kW, 50 mA, with Cu $K\alpha$ radiation. The instrument model was D/max-2550 X-ray diffractometer (Rigaku inc, Tokyo, Japan). The data of XRD were analyzed with JADE software (version 6.5, Jade, Christchurch, New Zealand). At the same time, the samples were characterized by scanning electron microscope (SEM SU6600, Hitachi High-Technology Corp., Tokyo, Japan) and transmission electron microscope (TEM JEOL 2100 F, JEOL Co., Ltd., Tokyo, Japan).

3. Results and Discussion

3.1. Structural Properties and Stability

Firstly, the structural stability of these $D0_{22}$ -type compounds was investigated. The crystal structure of the binary compound $D0_{22}$ - Al_3TM , where TM is Sc, Ti, V, Y, Zr, Nb, La, Hf, Ta, is displayed in Figure 1. The $D0_{22}$ -type compounds are tetragonal crystal with a space group of $I4/mmm$. Except for Al element, the composition of these compound elements is mainly composed of transition elements. Although these transition elements form the same crystal structure with aluminum, they have a greater impact on the properties of the compound. Being able to understand their internal mechanisms is very important for the design of alloys.

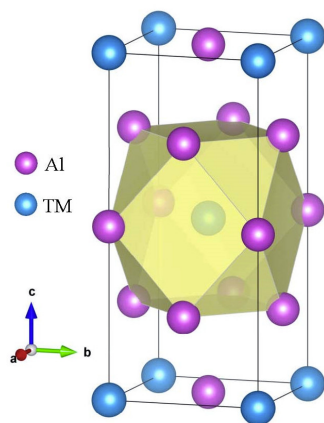


Figure 1. The crystal structure of $D0_{22}$ -type Al_3TM compounds.

In order to determine the phase stability of Al_3TM (TM = Sc, Ti, V, Y, Zr, Nb, La, Hf, Ta) intermetallics, the formation enthalpy and cohesive energy of these compounds are calculated by following equations [31,32]:

$$\Delta H = \frac{1}{x+y} \left(E_{\text{tot}} - xE_{\text{solid}}^{\text{A}} - yE_{\text{solid}}^{\text{B}} \right), \quad (1)$$

$$E_{\text{coh}} = \frac{1}{x+y} \left(E_{\text{tot}} - xE_{\text{atom}}^{\text{A}} - yE_{\text{atom}}^{\text{B}} \right), \quad (2)$$

where ΔH is the formation enthalpy of Al_3TM compound. E_{tot} is the total energy of Al_3TM phase. $E_{\text{solid}}^{\text{A}}$ and $E_{\text{solid}}^{\text{B}}$ are the energy of Al and TM atom, respectively. In addition, E_{coh} is the cohesive energy of Al_3TM compound. $E_{\text{atom}}^{\text{A}}$ and $E_{\text{atom}}^{\text{B}}$ is the energy of Al and TM free atom, respectively. The x and y are the number of Al and TM atom in the $\text{D0}_{22}\text{-Al}_3\text{TM}$ crystal structure, respectively. The calculated results of this work are noted in Table 1 and compared with other previous values [13,21,32,33]. The order of the compounds is arranged according to the atomic number of the TM atom in the periodic table of the elements. After analysis, it is evidence that the obtained results are basically coincident with the other calculated values, which indicates the reliability and good self-consistency of the proposed method.

Table 1. The calculated lattice constant (a , c in Å), density (ρ , g/cm^3), volume (Å^3), ΔH (eV/atom) and E_{coh} (eV/atom) of the Al_3TM compounds.

Species	Atomic Number	a	c	ρ	V	ΔH	ΔE
Al_3Sc	21	4.024	8.840	2.920	143.173	−0.366	−4.221
		4.021 [13]	8.822 [13]				
Al_3Ti	22	3.850	8.630	3.346	127.892	−0.396	−4.793
		3.851 [13]	8.576 [13]				
Al_3V	23	3.773	8.324	3.697	118.484	−0.283	−4.846
		3.766 [13]	8.312 [13]				
		3.773 [21]	8.325 [21]				
Al_3Y	39	4.194	9.260	3.464	162.863	−0.295	−4.178
Al_3Zr	40	3.963	9.027	4.034	141.757	−0.464	−4.916
Al_3Nb	41	3.854	8.641	4.497	128.382	−0.419	−5.473
		3.855 [21]	8.645 [21]				
Al_3La	57	4.454	9.240	3.984	183.279	−0.134	−3.934
Al_3Hf	72	3.946	8.918	6.206	138.842	−0.406	−4.906
		3.946 [33]	8.924 [33]				
Al_3Ta	73	3.862	8.591	6.789	128.121	−0.322	−5.151
		3.857 [34]	8.598 [34]				

The first principle calculation is carried out at the ground state of 0 K and 0 Pa. The formation enthalpy of the compound is negative, indicating that the formation of the compound is an exothermic process. The more negative the formation enthalpy, the more stable the compound is. It can be seen from Table 1 that the formation enthalpy of these nine D0_{22} -type compounds is less than zero, meaning that these compounds are thermodynamically stable in the ground state.

It is clear from Table 1 that the calculated value of cohesive energy of these compounds is −4.221, −4.793, −4.846, −4.178, −4.916, −5.473, −3.934, −4.906, −5.151 eV/atom for Al_3Sc , Al_3Ti , Al_3V , Al_3Y , Al_3Zr , Al_3Nb , Al_3La , Al_3Hf , Al_3Ta , respectively. Generally speaking, the large cohesive energy of compounds can only show that the free atoms of the two elements release more energy when they bond. If the energy needed to break the combination of the two elements is also large, the compound is still relatively unstable. However, the thermodynamic stability of compounds is affected by their enthalpy of formation. To some extent, the lower the enthalpy of formation, the easier the compounds are to form and the higher the thermodynamic stability [35,36]. The results show that the value of formation enthalpy of these D0_{22} -type compounds is −0.366, −0.396, −0.283, −0.295, −0.464, −0.419, −0.134, −0.406, −0.322 eV/atom for Al_3Sc , Al_3Ti , Al_3V , Al_3Y ,

Al_3Zr , Al_3Nb , Al_3La , Al_3Hf , Al_3Ta , respectively. The formation enthalpy of Al_3Zr is the lowest, which suggests that Al_3Zr alloy has the strongest formation ability and the most stable thermodynamics, while Al_3La is on the contrary. Therefore, the alloying ability of the nine D_{022} -type compounds from strong to weak can be arranged as $\text{Al}_3\text{Zr} > \text{Al}_3\text{Nb} > \text{Al}_3\text{Hf} > \text{Al}_3\text{Ta} > \text{Al}_3\text{Ti} > \text{Al}_3\text{Sc} > \text{Al}_3\text{V} > \text{Al}_3\text{Y} > \text{Al}_3\text{La}$, as showed in Figure 2. Considering all these compounds together, it is found that the Al_3Zr is the most thermodynamic stable compound.

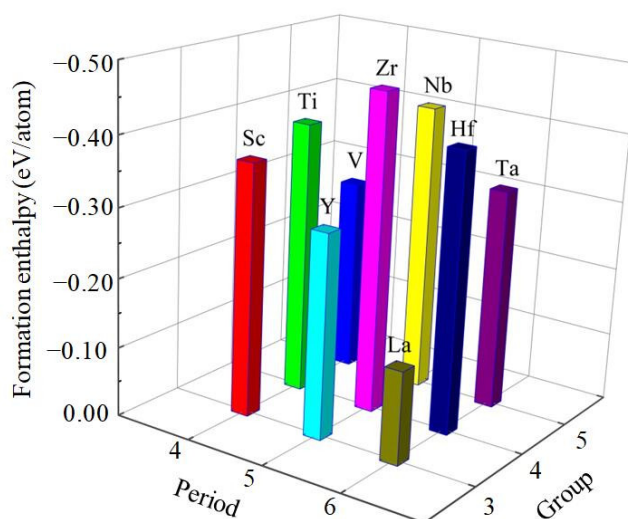


Figure 2. The calculated formation enthalpies of Al_3TM compounds.

3.2. Mechanical Stability, Elastic Properties and Moduli

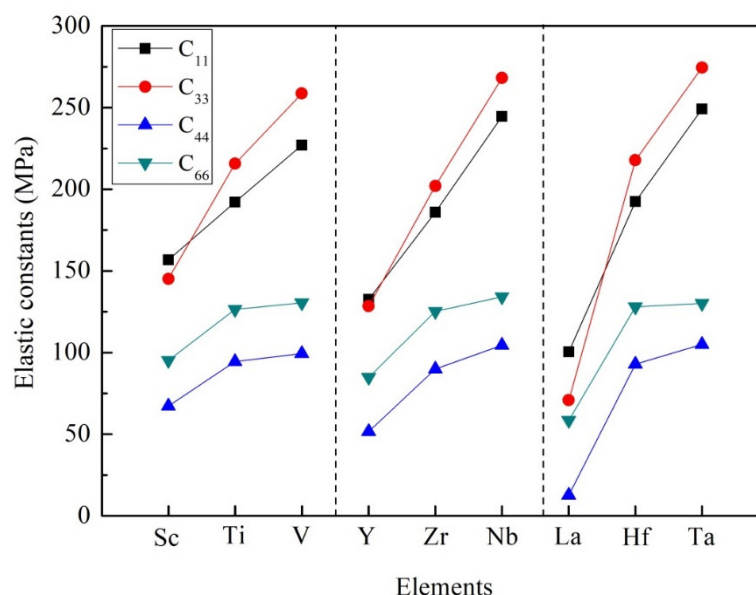
As well known, elastic constant is a very significant index to characterize the properties of compounds. The elastic constant is the index of material elasticity, which is related to the stress-strain relationship in the anisotropic medium. To some extent, the elastic constant also indicates the influence of crystal dynamics on mechanical behavior. The stress-strain method is used to calculate the elastic constants in the present calculation process and the results can be listed in Table 2. Furthermore, for the D_{022} -type crystal, tetragonal phase (C_{11} , C_{33} , C_{44} , C_{66} , C_{12} , and C_{13}) [37], the elastic constants can be restricted by the following Formula (3):

$$\begin{aligned} C_{11} > 0, C_{33} > 0, C_{44} > 0, C_{66} > 0 \\ (C_{11} - C_{12}) > 0, (C_{11} + C_{33} - 2C_{13}) > 0, \\ [2(C_{11} + C_{12}) + C_{33} + 4C_{13}] > 0. \end{aligned} \quad (3)$$

It is noticeable that the elastic constants calculated in Table 2 conform to the mechanical stability criterion. According to Equation (3), these D_{022} -type compounds are mechanically stable at 0 K. The elastic constants C_{11} , C_{22} , and C_{33} mean the compressibility of the crystal structure along the a-axis, b-axis, and c-axis, respectively. In the tetragonal system, C_{11} and C_{22} have the same value. Similarly, the value of C_{44} in the tetragonal system is the same as that of C_{55} . The value of C_{44} indicates the ability to resist shear strain in (100) or (010) plane, while the value of C_{66} represents the ability to resist shear strain in (001) plane. In view of Al_3Sc , Al_3Y and Al_3La compounds, the calculated value of C_{33} is less than that of C_{11} , which proves that the a-axis has greater compression resistance than the c-axis. However, for other compounds, such as Al_3Ti , Al_3V , Al_3Zr , Al_3Nb , Al_3Hf , Al_3Ta , the elastic constants of C_{33} are higher than that of C_{11} , suggesting that the c-axis has greater compression resistance than the a-axis, as illustrated in Figure 3. In particular, it was found that Al_3Ta has the highest resistance along the a-axis, b-axis, and c-axis. Besides, the values of C_{11} and C_{33} are larger than that of C_{44} and C_{66} . It means that these D_{022} -type phases are highly deformation resistant under uniaxial stress along the a- and c-axis.

Table 2. The calculated elastic constants C_{ij} (GPa) of Al_3TM compounds.

Species	C_{11}	C_{12}	C_{13}	C_{33}	C_{44}	C_{66}
Al_3Sc	156.86	56.88	42.17	145.14	67.20	95.17
	158.00 [13]	60.00 [13]	42.00 [13]	158.00 [13]	63.00 [13]	93.00 [13]
Al_3Ti	192.06	84.53	44.60	215.66	94.46	126.42
	192.00 [13]	84.00 [13]	49.00 [13]	216.00 [13]	94.00 [13]	122.00 [13]
Al_3V	227.01	89.03	45.95	258.69	99.37	130.55
	233.00 [13]	77.00 [13]	47.00 [13]	258.00 [13]	104.00 [13]	129.00 [13]
	220.87 [21]	92.69 [21]	45.26 [21]	256.95 [21]	98.57 [21]	130.25 [21]
Al_3Y	132.51	58.63	38.77	128.45	51.60	84.84
Al_3Zr	185.96	85.34	43.13	202.08	90.00	125.22
Al_3Nb	244.54	92.28	45.94	268.13	104.57	134.22
	242.57 [21]	92.85 [21]	45.78 [21]	266.84 [21]	102.41 [21]	134.03 [21]
Al_3La	100.51	55.51	39.49	70.85	12.67	58.57
Al_3Hf	192.46	88.32	48.29	217.76	92.91	127.96
	193.60 [33]	87.10 [33]	47.40 [33]	217.80 [33]	92.40 [33]	123.30 [33]
Al_3Ta	249.05	88.99	52.89	274.55	104.96	130.05

**Figure 3.** The trend of elastic constants of Al_3TM compounds.

On the other hand, the bulk modulus (B), shear modulus (G), Young's modulus (E) and Poisson's ratio (σ) of Al_3TM crystal can be calculated by Voigt-Reuss-Hill (VRH) approximation method. Using the following formulas [38], the calculated values are shown in Table 3.

$$B_H = \frac{1}{2}(B_V + B_R), \quad (4)$$

$$G_H = \frac{1}{2}(G_V + G_R), \quad (5)$$

$$E = \frac{9B_H G_H}{(3B_H + G_H)}, \quad (6)$$

$$\sigma = \frac{(3B_H - 2G_H)}{[2(3B_H + G_H)]}, \quad (7)$$

where the subscript symbols H denotes the modulus values obtained by the Hill approximation. The subscript V and R mean the modulus values obtained by the Voigt and Reuss approximation methods, respectively. Furthermore, the Voigt approximation limits the maximum of elastic modulus and the Reuss approximation is considered to be the

minimum of elastic modulus. The Hill approximation uses the average value of Voigt and Reuss to express the elastic constants of materials.

Table 3. The calculated bulk modulus (GPa), shear modulus (GPa), Young's modulus (GPa), B/G, Poisson's ratio and Vickers hardness (GPa) of Al_3TM compounds.

Species	B_V	B_R	B	G_V	G_R	G	E	σ	B/G	Hv
Al_3Sc	82.37	81.91	82.14	67.09	63.88	65.49	155.21	0.185	1.25	14.72
Al_3Ti	92.1 [25]	91.8 [25]	84.00 [13]	74.1 [25]	71.7 [25]	72.9 [25]	173.1 [25]	0.19 [25]	1.26 [25]	19.32
	105.25	105.14	105.19	91.47	84.71	88.09	206.60	0.173	1.19	
Al_3V	102.4 [25]	102.2 [25]	107.00 [13]	81.8 [25]	81.7 [25]	81.8 [25]	193.8 [25]	0.18 [25]	1.25 [25]	20.70
	119.40	119.35	119.37	101.31	97.05	99.18	233.01	0.175	1.20	
Al_3Y	73.98	73.55	118.00 [13]	54.76	50.91	97.22 [21]	228.95 [21]	0.178 [21]	1.217 [21]	10.78
	101.91	101.61	118.32 [21]	87.87	80.58	52.83	127.95	0.211	1.40	
Al_3Zr	100.8 [25]	100.6 [25]	101.76	84.6 [25]	83.3 [25]	84.23	198.04	0.176	1.21	18.45
	125.06	124.89	100.7 [25]	106.88	103.25	84.0 [25]	197.2 [25]	0.17 [25]	1.20 [25]	
Al_3Nb	125.06	124.89	124.98	106.88	103.25	105.06	246.20	0.172	1.19	21.85
			124.45 [21]			103.71 [21]	243.50 [21]	0.174 [21]	1.200 [21]	
Al_3La	60.09	56.78	58.43	25.94	18.88	22.41	59.62	0.330	2.61	1.02
	108.05	107.96	108.01	90.61	83.30	86.95	205.67	0.183	1.24	
Al_3Hf	106.5 [25]	106.0 [25]	106.3 [25]	77.8 [25]	77.4 [25]	77.6 [25]	187.2 [25]	0.21 [25]	1.37 [25]	18.15
			107.60 [33]			86.60 [33]	204.80 [33]	0.180 [33]	1.24 [33]	
Al_3Ta	130.22	130.18	130.21	109.53	106.85	108.19	254.17	0.175	1.20	21.94

It is noted that the calculated values of elastic moduli are summarized in the Table 3. Obviously, the bulk modulus of these D0_{22} -type compounds decreased in order: $\text{Al}_3\text{Ta} > \text{Al}_3\text{Nb} > \text{Al}_3\text{V} > \text{Al}_3\text{Hf} > \text{Al}_3\text{Ti} > \text{Al}_3\text{Zr} > \text{Al}_3\text{Sc} > \text{Al}_3\text{Y} > \text{Al}_3\text{La}$, as shown in Figure 4. The bulk modulus of crystal reflects the resistance of crystal under water pressure. At the microscopic level, the bulk modulus of the crystal is determined by the strength of the chemical bond. The larger the bulk modulus of the crystal, the stronger the chemical bond strength and the stronger the compression resistance. The calculated results show that Al_3Ta has the strongest resistance of compression. Oppositely, Al_3La has the weakest resistance of compression.

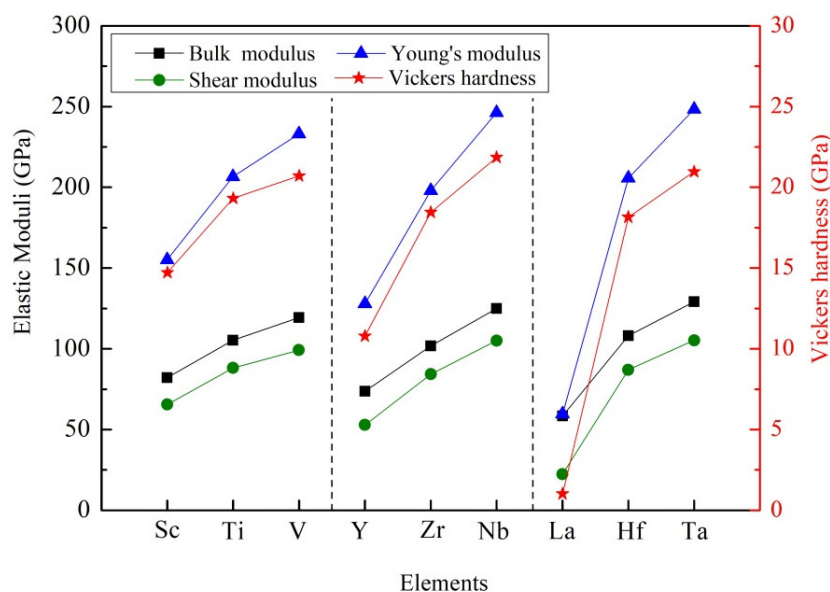


Figure 4. Comparison of moduli and Vickers hardness of different compounds.

Generally, shear modulus refers to the ability of a material to resist shear strain. The higher the shear modulus, the stronger the rigidity of the material. As listed in Table 3,

Al_3Ta and Al_3La have the largest shear modulus (108.19 GPa) and smallest one (22.41 GPa), respectively. At the same time, Young's modulus is a term of material mechanics, which is used to express the deformation resistance of solid materials. The rigidity of the material can be reflected by the value of Young's modulus. That is to say, the greater the Young's modulus is, the greater the rigidity of the material is, and the harder it is to deform. It can be seen that Al_3Ta and Al_3La have the largest Young's modulus (254.17 GPa) and smallest one (59.62 GPa). It is evident that Al_3Ta has the greater rigidity and is difficult to deform.

Furthermore, the brittleness and ductility of the materials can be judged by Poisson's ratio. This is due to Poisson's ratio being the ratio of transverse strain to longitudinal strain when the material is deformed under tension or compression. A value of 0.26 is taken as the critical value of brittle and plastic separation. When the value of Poisson's ratio is greater than 0.26, it can be considered as ductile material. On the contrary, it can be determined as brittle material.

When the value of Poisson's ratio is less than 0.26, it can be judged as brittle material. Otherwise, it can be judged as ductile material [39,40]. As for these D0_{22} -type compounds, the Poisson's ratios are 0.185, 0.173, 0.175, 0.211, 0.176, 0.172, 0.183, and 0.175 for Al_3Sc , Al_3Ti , Al_3V , Al_3Y , Al_3Zr , Al_3Nb , Al_3Hf , and Al_3Ta respectively, while the Poisson's ratio of Al_3La is 0.330. Therefore, it is noted that Al_3La shows toughness and the other eight compounds exhibit brittle property. Similarly, brittleness and ductility of compounds can be predicted by the ratio of bulk modulus to shear modulus [41,42]. Based on the Pugh standard, the material presents brittleness when the value of B/G is less than 1.75, otherwise the material exhibit toughness. As can be shown in Table 3 that the B/G of Al_3Sc , Al_3Ti , Al_3V , Al_3Y , Al_3Zr , Al_3Nb , Al_3Hf , and Al_3Ta is less than 1.75, indicating that these eight D0_{22} -type compounds are brittle. On the contrary, the B/G value of Al_3La is greater than 1.75, which shows toughness.

Ultimately, it is reported that the hardness of a compound is directly related to its shear modulus and Young's modulus. At present, although the accurate relationship between hardness and elastic modulus has not been determined, the larger elastic modulus can represent the higher hardness. For the nine compounds studied, their Vickers hardness (H_V) of Al_3TM -type compounds can be forecasted by the following empirical formula [43]:

$$H_V = 2 \left(G^3 / B^2 \right)^{0.585} - 3, \quad (8)$$

As presented in Table 3, the maximum Vickers hardness of Al_3TM is Al_3Ta , which is 21.94 GPa. The minimum Vickers hardness is Al_3La and its value is 1.02 GPa. Similar trends indicate that Al_3Ta and Al_3La have the largest Young's modulus and smallest one, as indicated in Figure 4. It is also confirmed that Young's modulus has a decisive effect on the hardness of the compound.

3.3. Mechanical Anisotropy

It is very important to study the anisotropy of D0_{22} -type compounds since this index has influence on the macroscopic mechanical properties of the alloy. In the present calculation, the universal anisotropic index (A^U), the percent anisotropy index (A_B and A_G) and the shear anisotropic factors (A_1 , A_2 and A_3) are estimated by the following expressions [44]:

$$A^U = 5 \frac{G_V}{G_R} + \frac{B_V}{B_R} - 6 \geq 0, \quad (9)$$

$$A_B = \frac{B_V - B_R}{B_V + B_R} \times 100\%, \quad (10)$$

$$A_G = \frac{G_V - G_R}{G_V + G_R} \times 100\%, \quad (11)$$

$$A_1 = \frac{4C_{44}}{C_{11} + C_{33} - 2C_{13}} \text{ for } (100) \text{ plane}, \quad (12)$$

$$A_2 = \frac{4C_{55}}{C_{22} + C_{33} - 2C_{23}} \text{ for (010) plane,} \quad (13)$$

$$A_3 = \frac{4C_{66}}{C_{11} + C_{22} - 2C_{12}} \text{ for (001) plane.} \quad (14)$$

The generated universal anisotropic index (A^U), percent anisotropy (A_B and A_G) and shear anisotropic factors (A_1 , A_2 and A_3) of these $D0_{22}$ -type compounds are exhibited in Table 4. The anisotropy of $D0_{22}$ -type compounds can be directly reflected by the value of A^U . In case of A^U is equal to zero, the crystal is isotropic. The larger the value of A^U , the stronger the anisotropy, and vice versa. It is noted that the values of A^U of Al_3Sc , Al_3Ti , Al_3V , Al_3Y , Al_3Zr , Al_3Nb , Al_3La , Al_3Hf , Al_3Ta are 0.257, 0.400, 0.220, 0.385, 0.455, 0.177, 1.927, 0.440, and 0.126, respectively. In this case, the anisotropic properties of these $D0_{22}$ -type compounds can be listed as $Al_3La > Al_3Zr > Al_3Hf > Al_3Ti > Al_3Y > Al_3Sc > Al_3V > Al_3Nb > Al_3Ta$.

Table 4. The calculated universal anisotropic index (A^U), percent anisotropy (A_B and A_G) and shear anisotropic factors (A_1 , A_2 and A_3) of Al_3TM compounds.

Species	A^U	A_B	A_G	A_1	A_2	A_3
Al_3Sc	0.257	0.282	2.448	1.235	1.235	1.904
Al_3Ti	0.400	0.053	3.838	1.186	1.186	2.351
Al_3V	0.220	0.019	2.149	1.009	1.009	1.892
Al_3Y	0.385	0.294	3.648	1.125	1.125	2.297
Al_3Zr	0.455	0.148	4.328	1.193	1.193	2.489
Al_3Nb	0.177	0.067	1.727	0.994	0.994	1.763
Al_3La	1.927	2.839	15.745	0.549	0.549	2.603
Al_3Hf	0.440	0.043	4.203	1.185	1.185	2.457
Al_3Ta	0.126	0.015	1.238	1.005	1.005	1.625

When the values of A_B and A_G are not equal to zero, it shows that the bulk modulus and shear modulus of the crystal are anisotropic. The values of A_B and A_G correspond to the anisotropy. It reveals that Al_3La has the largest A_B value 2.839, indicating that the bulk modulus anisotropy of Al_3La is the strongest. Then, the bulk modulus anisotropy of Al_3Y , Al_3Sc , Al_3Zr , Al_3Nb , Al_3Ti , Al_3Hf , Al_3V , and Al_3Ta decrease gradually. Evidently, The A_G value of Al_3La is the highest and that of Al_3Ta is the lowest, indicating that Al_3La and Al_3Ta have the strongest and weakest shear modulus anisotropy, respectively.

Furthermore, the shear factors A_1 , A_2 , and A_3 can be used to represent anisotropy on (100), (010), and (001) planes. When the values of A_1 , A_2 , and A_3 are 1, the crystal is isotropic. According to the calculated results, all $D0_{22}$ -type compounds have different degrees of elastic anisotropy, as noted in the Table 4. Among these $D0_{22}$ -type phases, the A_1 (A_2) values of Al_3La deviate most severely from 1, which imply that Al_3La exhibits the strongest shear anisotropy in (100) and (010) planes. Conversely, the values of A_1 (A_2) of Al_3Ta have the least deviation among these $D0_{22}$ -type compounds, which mean that the Al_3Ta exists the lowest shear anisotropy in the (100) plane and (010) plane. The A_3 value of Al_3La has the most deviation from 1, hinting that the Al_3La shows the highest shear anisotropy in the (001) plane. These $D0_{22}$ -type phases all have a wide deviation from 1 in the (001) plane.

On the other hand, the three-dimensional (3D) image has the characteristics of clear hierarchy and visual intuition, which can show the anisotropic characteristics of these $D0_{22}$ -type compounds more clearly and vividly. In this study, bulk modulus, shear modulus, and Young's modulus of different $D0_{22}$ -type compounds are drawn with spherical coordinates. The relationship between bulk modulus, shear modulus, Young's modulus, and different directions can be realized by the following formulas [45,46]:

$$\frac{1}{B} = (S_{11} + S_{12} + S_{13}) \left(l_1^2 + l_2^2 \right) + (2S_{13} + S_{33}) l_3^2, \quad (15)$$

$$\frac{1}{G} = \frac{1}{2}(S_{66} + S_{44}) + (4S_{11} - 4S_{12} - 2S_{66})l_1^2l_2^2 + (2S_{11} + 2S_{33} - 4S_{13} - 2S_{44})(l_1^2l_3^2 + l_2^2l_3^2) + \frac{1}{2}(S_{44} - S_{66})l_3^4, \quad (16)$$

$$\frac{1}{E} = S_{11}(l_1^4 + l_2^4) + (2S_{13} + S_{44})(l_1^2l_3^2 + l_2^2l_3^2) + S_{33}l_3^4 + (2S_{12} + S_{66})l_1^2l_2^2, \quad (17)$$

where, $l_1 = \sin\theta\cos\phi$, $l_2 = \sin\theta\sin\phi$, $l_3 = \cos\theta$, l_1 , l_2 and l_3 the directional cosines, S_{ij} the elastic compliance constants. If the system is isotropic, the three-dimensional directional correlation is spherical. The deviation of spherical shape suggests the degree of anisotropy.

It is clear from the 3D stereoscopic pictures of bulk modulus, shear modulus, and Young's modulus that D0₂₂-type compounds with the same crystal structures and different compositions reveal different degree anisotropies. It can also be seen from Figure 5 that the bulk modulus of Al₃La shows the strongest anisotropy. This result is consistent with the maximum anisotropy index A_B of Al₃La calculated in Table 4. As proved in Figure 6, the shear modulus anisotropy of Al₃La is the strongest, while that of Al₃Ta is the weakest. This phenomenon is consistent with the results obtained by the anisotropy index A_C in Table 4. Finally, the anisotropic properties of Young's modulus of these D0₂₂-type compounds can be arranged as Al₃La > Al₃Zr > Al₃Hf > Al₃Ti > Al₃Y > Al₃Sc > Al₃V > Al₃Nb > Al₃Ta, as noted in Figure 7.

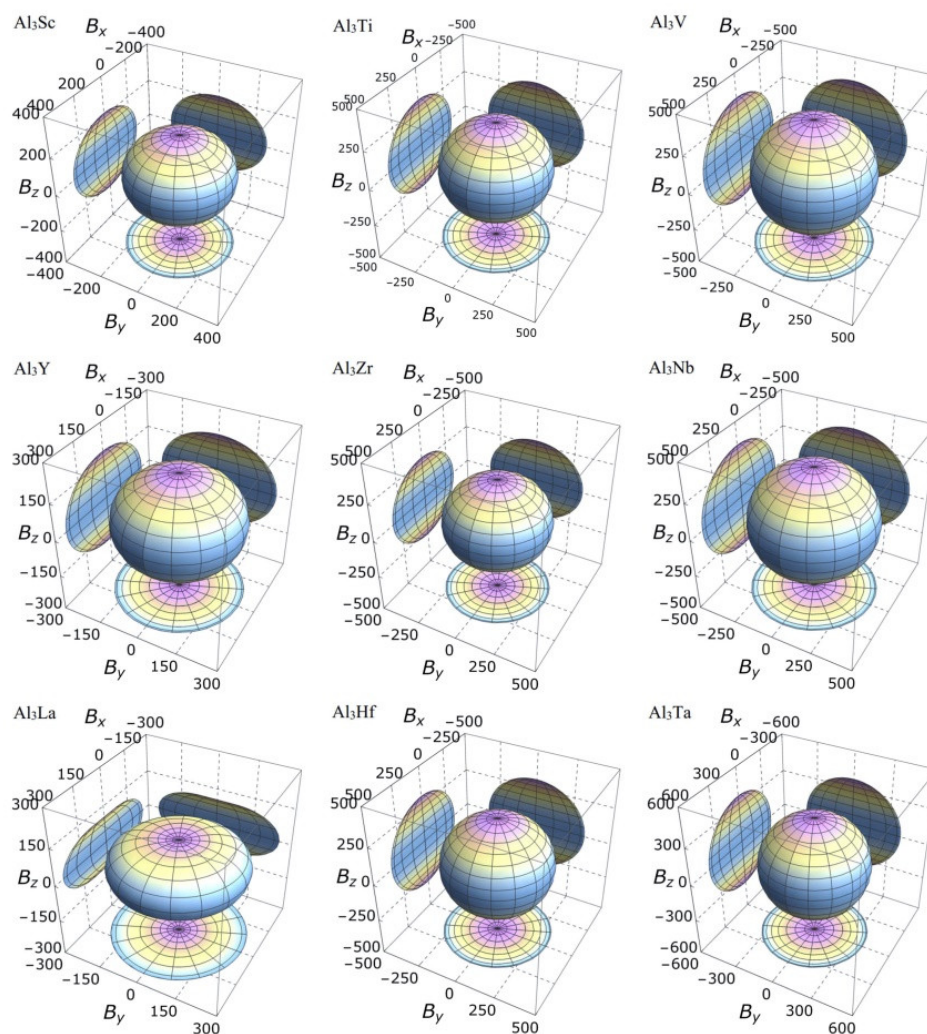


Figure 5. The anisotropic characteristics of bulk modulus of the Al₃TM compounds.

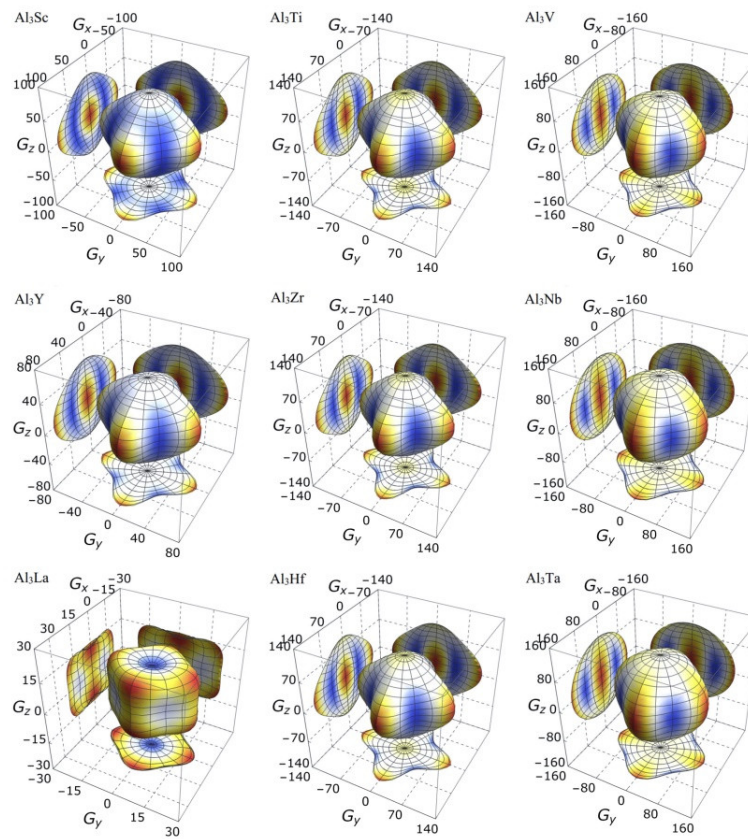


Figure 6. The anisotropic characteristics of shear modulus of the Al_3TM compounds.

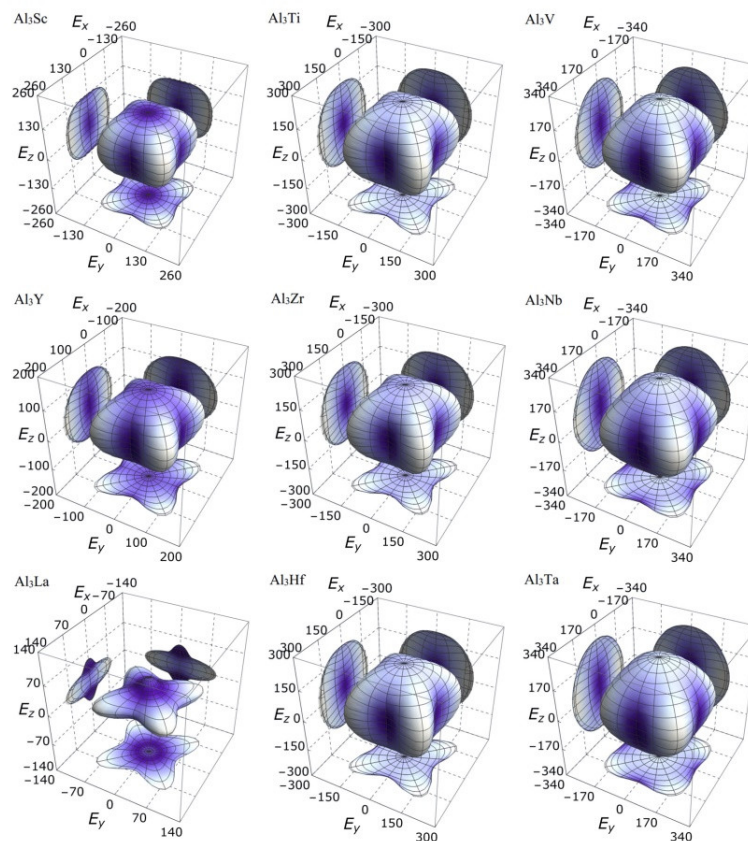


Figure 7. The anisotropic characteristics of Young's modulus of the Al_3TM compounds.

In particular, the projecting images of bulk modulus, shear modulus, and Young's modulus can display the anisotropy details of the compounds more clearly, which are given in Figure 8. It should be noted that the projection features of (100) and (010) crystal planes are the same, so only the projections of (001), (010), and (110) plane are listed here. Obviously, the bulk modulus of these compounds shows greater anisotropic on the (010) and (100) planes, but it exhibits isotropy on the (001) plane. The degree of anisotropy of the same compound on (010) and (100) is the same, suggesting that the order of anisotropy is $\text{Al}_3\text{La} > \text{Al}_3\text{Y} > \text{Al}_3\text{Sc} > \text{Al}_3\text{Zr} > \text{Al}_3\text{Nb} > \text{Al}_3\text{Ti} > \text{Al}_3\text{Hf} > \text{Al}_3\text{V} > \text{Al}_3\text{Ta}$. Additionally, the shear moduli of these D_{022} -type compounds are anisotropic on all three planes. Especially, the 3D diagram morphology of Al_3La shear modulus anisotropy is different from that of the other eight compounds. These eight compounds have the similar anisotropy on the (001) crystal plane, while the anisotropy degree of Al_3Ta displays the lowest. Furthermore, among these eight compounds, the anisotropy of Al_3Ta in three crystal faces (001), (010), and (100) is smaller. Similarly, the Young's moduli of the nine compounds are anisotropic in three planes. The degree of anisotropy of Al_3Ti , Al_3V , Al_3Y , Al_3Zr , Al_3Nb , Al_3Hf , and Al_3Ta is smaller on (100) and (010) crystal planes, while that of Al_3Sc and Al_3La is larger on (100) and (010) crystal planes. However, it is interesting to note that the anisotropy of Young's modulus is in the opposite direction to that of the shear modulus. Obviously, the Young's modulus of Al_3Ta is less anisotropic in all three planes, while the anisotropy of Al_3La is greater.

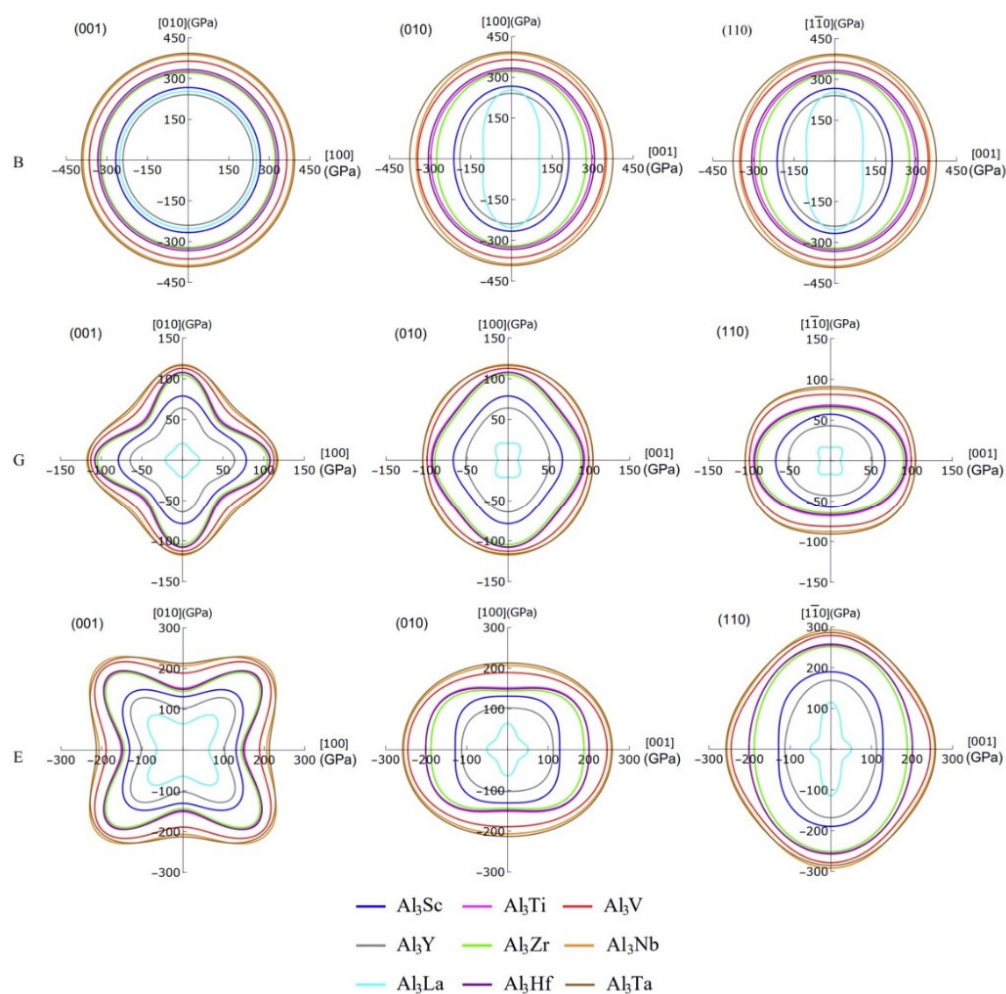


Figure 8. The projections of bulk modulus, shear modulus and Young's modulus on the (001), (010), and (110) crystal planes of Al_3TM compounds.

Strangely, from Figures 5–8, the anisotropic appearances of Al₃La in bulk modulus, shear modulus, and Young's modulus is quite different from those of the other eight compounds. As discussed earlier, Al₃La has higher enthalpy of formation, lower modulus values, unique toughness, and smallest Vickers hardness. Thus, it is speculated that D0₂₂-type Al₃La may not exist.

Corresponding to Figure 8, the Table 5 summarizes more specific values of bulk modulus, shear modulus, and Young's modulus in four directions. Due to the structural properties of D0₂₂-type compounds, the bulk modulus, shear modulus, and Young's modulus are equal in the directions of [100] and [010]. Likewise, the bulk modulus of these compounds in the $[\bar{1}\bar{1}0]$ direction is equal to those in the [100] and [010] directions. However, the shear modulus and Young's modulus of these compounds in the $[\bar{1}\bar{1}0]$ direction are not equal to those in the [100] and [010] directions. The maximum and minimum bulk modulus of Al₃Ta and Al₃La in [001] direction is 375.16 and 103.00 GPa, respectively. This means that Al₃Ta has the strongest resistance of compression in [001] direction. In addition, the shear modulus in the directions of [001] and $[\bar{1}\bar{1}0]$ are smaller than those in the directions of [100] and [010], which indicates stronger shear strain capacity. The maximum shear modulus of Al₃Nb in [100] and [010] direction is 117.56 GPa. Furthermore, the Young's modulus of other compounds except Al₃Sc and Al₃La in the [001] direction is greater than that in the [100] and [010] directions. The reason is that the C₃₃ value of Al₃Sc and Al₃La is smaller than C₁₁ and C₂₂, which leads to greater compressibility in c-axis direction.

Table 5. The calculated uniaxial elastic moduli (GPa) in different directions of Al₃TM compounds.

Species	B				G				E			
	[100]	[010]	[001]	$[\bar{1}\bar{1}0]$	[100]	[010]	[001]	$[\bar{1}\bar{1}0]$	[100]	[010]	[001]	$[\bar{1}\bar{1}0]$
Al ₃ Sc	266.74	266.74	212.26	266.74	78.78	78.78	67.20	57.33	130.84	130.84	128.50	189.79
Al ₃ Ti	325.45	325.45	297.08	325.45	108.13	108.13	94.46	68.53	151.81	151.81	201.28	255.45
Al ₃ V	364.46	364.46	345.91	364.46	112.85	112.85	99.37	81.44	188.96	188.96	245.33	279.07
Al ₃ Y	240.26	240.26	189.66	240.26	64.17	64.17	51.60	43.06	102.58	102.58	112.72	168.70
Al ₃ Zr	321.50	321.50	276.17	321.50	104.73	104.73	90.00	64.54	143.97	143.97	188.37	251.67
Al ₃ Nb	387.46	387.46	351.47	387.46	117.56	117.56	104.57	88.11	206.57	206.57	255.60	292.41
Al ₃ La	253.02	253.02	103.00	253.02	20.84	20.84	12.67	16.21	64.20	64.20	50.86	114.52
Al ₃ Hf	333.26	333.26	306.61	333.26	107.66	107.66	92.91	66.74	148.61	148.61	201.15	257.63
Al ₃ Ta	393.05	393.05	375.16	393.05	116.16	116.16	104.96	90.85	212.90	212.90	257.95	285.91

3.4. Electronic Structures

The compounds in present work are all D0₂₂-type compounds that are bound with transition metals. Because of their orientation-related bonding properties, it is of great significance to analyze the chemical bonding properties and electronic structures of these D0₂₂-type compounds. In Figure 9, we calculated the total density of states (TDOS) and partial density of states (PDOS) of D0₂₂-Al₃TM compounds. The vertical dashed line at zero energy shows the Fermi level (E_F). Obviously, the density of states at Fermi level is not zero, suggesting that these phases have metal properties and electrical conductivity. For Al₃Sc, Al₃Ti, Al₃V, Al₃Y, Al₃Zr, Al₃Nb, Al₃La, Al₃Hf, and Al₃Ta phases, there is a peak near the Fermi level of the TDOS curves, implying their good conductivity.

It is obvious that the TDOS at the Fermi level for Al₃Sc, Al₃Ti, Al₃V, Al₃Y, Al₃Zr, Al₃Nb, Al₃La, Al₃Hf and Al₃Ta are 3.43, 4.25, 1.99, 3.59, 3.85, 1.30, 4.65, 3.71, and 1.08 electrons/eV, respectively. The TDOS curve in Figure 9 also shows the pseudogap near E_F, which is due to the electron transfer to the low energy region. The lower the position of E_F in the gap, the more stable the structure of intermetallics is. Thus, Al₃Ta can be considered as the most stable compound. When the pseudogap is larger, it means stronger bond strength and higher deformation resistance. Compared with Al₃V, Al₃Nb, and Al₃Ta in Figure 9, it can be noted that the pseudogap of Al₃Ta has the widest gap, meaning that the covalent bond strength of Al₃Ta is stronger than that of Al₃V and Al₃Nb. This explains why Al₃Ta has

the highest hardness. In view of nine compounds, the shapes of TDOS for Al_3Sc , Al_3Ti , Al_3Y , Al_3Zr , Al_3La , and Al_3Hf are similar, which demonstrate that their chemical bonds are similar. The TDOS curves of Al_3V , Al_3Nb , and Al_3Ta are alike, which is to say that the V-shaped tip intersects the dotted line of Fermi level.

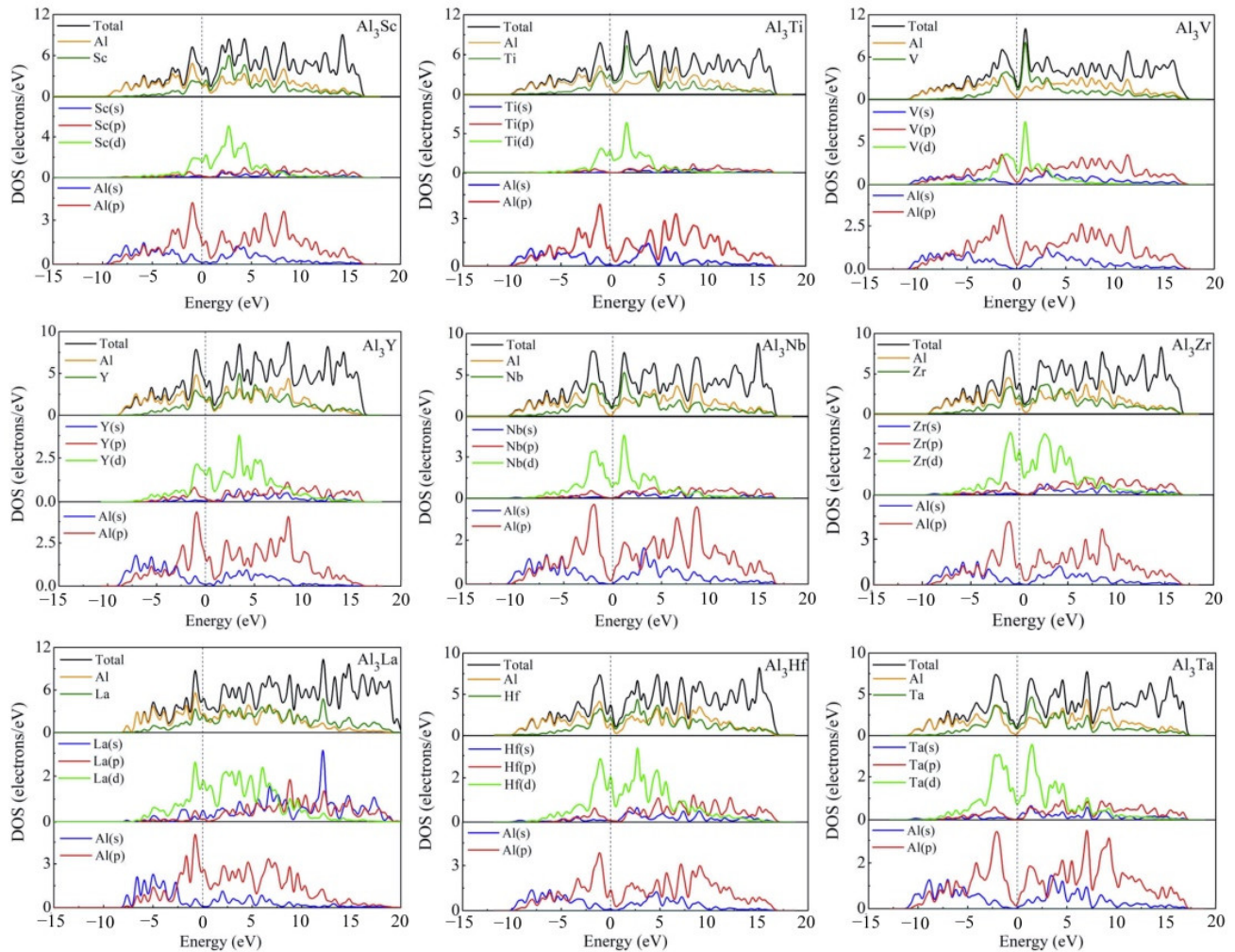


Figure 9. Total and partial electronic densities of states near Fermi level of Al_3TM compounds.

The PDOS curves clearly show that the contribution of Al-s on the surface of Fermi level is small, which is mainly contributed by the Al-p state. The Fermi level of TDOS is mainly formed by the strong hybridization of Al-p and TM (TM = Sc, Ti, V, Y, Zr, Nb, La, Hf, Ta)-d states. Obviously, the hybridization of Al-s and TM (TM = Sc, Ti, V, Y, Zr, Nb, La, Hf, Ta)-s states are less helpful for the Fermi level of TDOS. The obtained quantity of bonding electrons per atom between -13 eV and Fermi level is 3.005, 3.243, 3.493, 3.003, 3.242, 3.499, 2.997, 3.247, and 3.501 for Al_3Sc , Al_3Ti , Al_3Y , Al_3V , Al_3Zr , Al_3Nb , Al_3La , Al_3Hf and Al_3Ta , respectively.

Meanwhile, in order to explore the chemical bonds and charge transfer in all D0_{22} -type compounds, the charge density difference on the (010) basal plane of these compounds were considered. In Figure 10, the distribution state of charge density difference of Al_3Sc , Al_3Ti , Al_3V , Al_3Y , Al_3Zr , Al_3Nb , Al_3La , Al_3Hf , and Al_3Ta can be seen clearly. The values of charge density difference map are plotted from -0.04 to 0.04 $\text{e}/\text{\AA}^3$. Besides, the red and blue mean separately the aggregation and reduction of electrons.

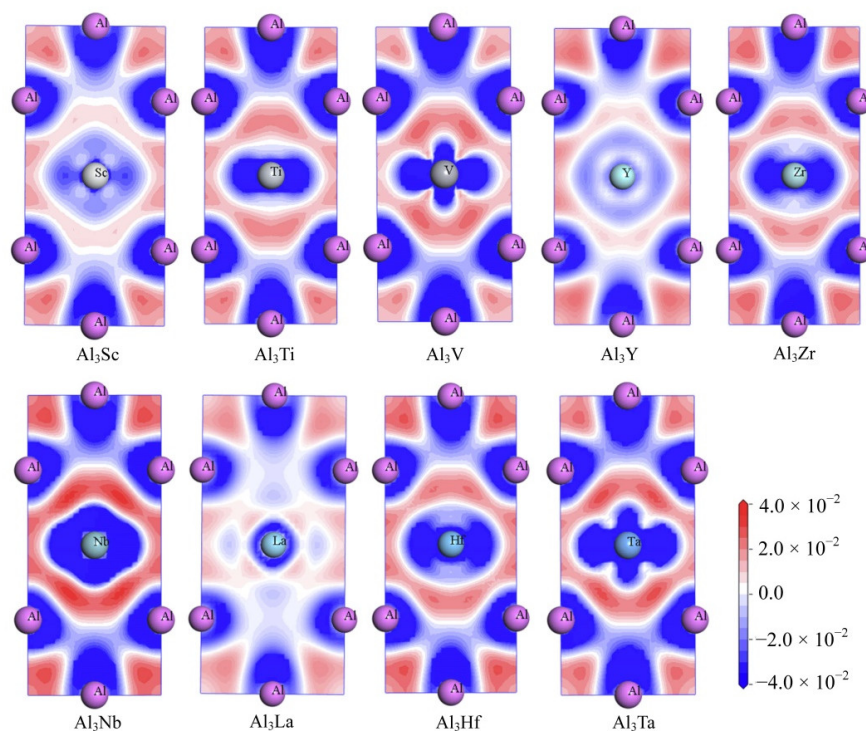


Figure 10. The electron density difference of Al_3TM compounds.

As can be seen from the Figure 10, there are electron deletions around both Al and TM atoms (blue), and electron aggregation between Al and TM atoms (red). This suggests that the electrons are aggregated into a covalent Al-TM bond between the atoms Al and TM. Similarly, there is a large amount of charge accumulation between Al and Al atoms, indicating that the Al-Al bond in the compound has covalent bond characteristics. Furthermore, a larger degree of localization of electrons reflects a stronger bond. Consequently, the electron concentration between the Al and TM (V, Nb and Ta) atoms in Al_3V , Al_3Nb and Al_3Ta compounds is higher, which leads to the conclusion that Al-TM (V, Nb and Ta) bonds are stronger. On the contrary, it can be suggested that the bonds of Al-La and La-La are the weakest, which is because the less the localization degree of electrons, the weaker the bonds are.

3.5. Work Function

In order to further understand the properties of D0_{22} -type compounds in this study, some surface work functions were calculated. Theoretically, the work function is the energy barrier used to move electrons from the surface of solid compounds to the free space, as noted by the following expression [47,48]:

$$\varphi = V_{\text{vac}} - E_{\text{F}}, \quad (18)$$

where φ is work function, and symbol V_{vac} means the electrostatic potential of the vacuum region near the surface. E_{F} corresponds to the Fermi energy of the slab. The schematic diagram of the electronic movement is presented in Figure 11. When a compound has a higher electron work function, it takes more energy to change its electron state. Therefore, there are greater obstacles to improving the state or properties of compounds such as mechanical and elastic properties. The higher electron work function of the compound indicates that it has stronger atomic bond [49,50]. In present work, the work function value of Al_3Sc , Al_3Ti , Al_3V , Al_3Y , Al_3Zr , Al_3Nb , Al_3La , Al_3Hf , and Al_3Ta is 3.838, 4.305, 4.206, 3.754, 3.953, 4.100, 3.291, 4.079, and 4.078 eV on (100) plane, respectively. It is found that the value of Al_3La is the smallest. Therefore, the Young's modulus and Vickers hardness of Al_3La are the lowest, which is consistent with the previous calculated results.

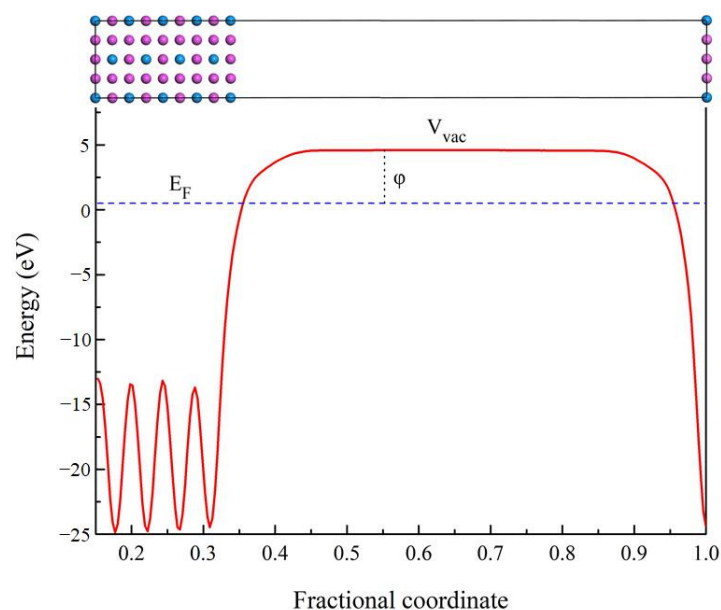


Figure 11. The schematic diagram of the electronic movement related to work function.

3.6. Experimental Design

Figure 12a shows the SEM and XRD images of representative CoCrFeAlTa_{0.16} HEA at 50 h annealing state. It is obvious that the alloy exhibits the crystal structure of FCC. The grain distribution in the image is clearly angular. The typical stress-strain curves of the solid solution and different heat treatment states can be seen in Figure 12b. It can be observed that the strength and toughness of the sample is better when it is treated at 700 °C/50 h. However, the strength and toughness of the samples were reduced when they were treated for 700 °C/100 h. It is possible that the grain size will be further enlarged as the solution time increases. In fact, the specimen annealed for 50 h will have D0₂₂-type Al₃Ta phase, resulting in its tensile strength up to 1120 MPa and elongation up to 26%. This result fully reflects the strengthening effect of Al₃Ta phase.

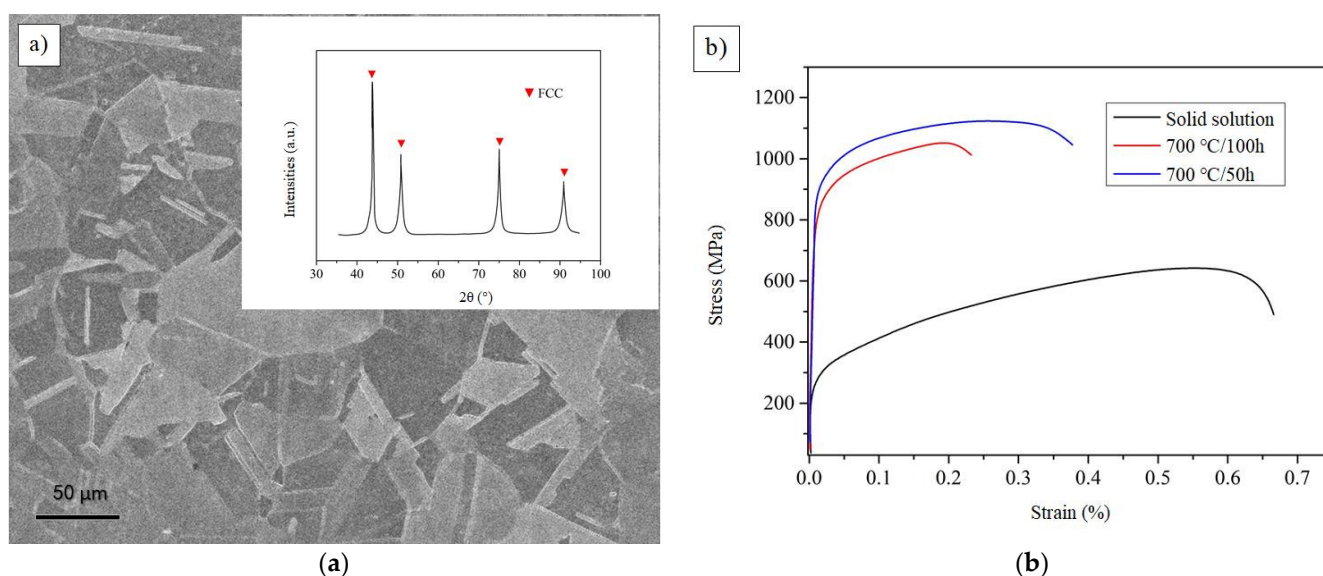


Figure 12. The SEM, XRD, and stress-strain curves of CoCrFeAlTa_{0.16}. (a) The SEM and XRD images at 50 h annealing state; (b) The stress-strain curves of different heat treatment states.

In order to more clearly characterize the microstructure of $D0_{22}$, Figure 13 exhibits the TEM structure of Al_3Ta phase. According to the image, the Al_3Ta phase is needle like and has a certain orientation. It presents a crystallographic relationship with the matrix, $[001]_{D0_{22}} // [001]_{Matrix}$. The diffraction pattern in Figure 13b clearly illustrates this relationship. It can be seen that plane $(\bar{2}20)$ of the matrix corresponds to plane (110) of $D0_{22}$ -type Al_3Ta phase. Moreover, stereographic projection of the orientation relationship denotes the crystal plane correspondence between the two phases more clearly, as shown in Figure 13c,d. This orientation relationship further indicates that the formation of Al_3Ta contributes to the improvement of its strength and toughness. Therefore, the reliability of the simulation is further confirmed by the experiments, which has important reference values for the design and application of this material.

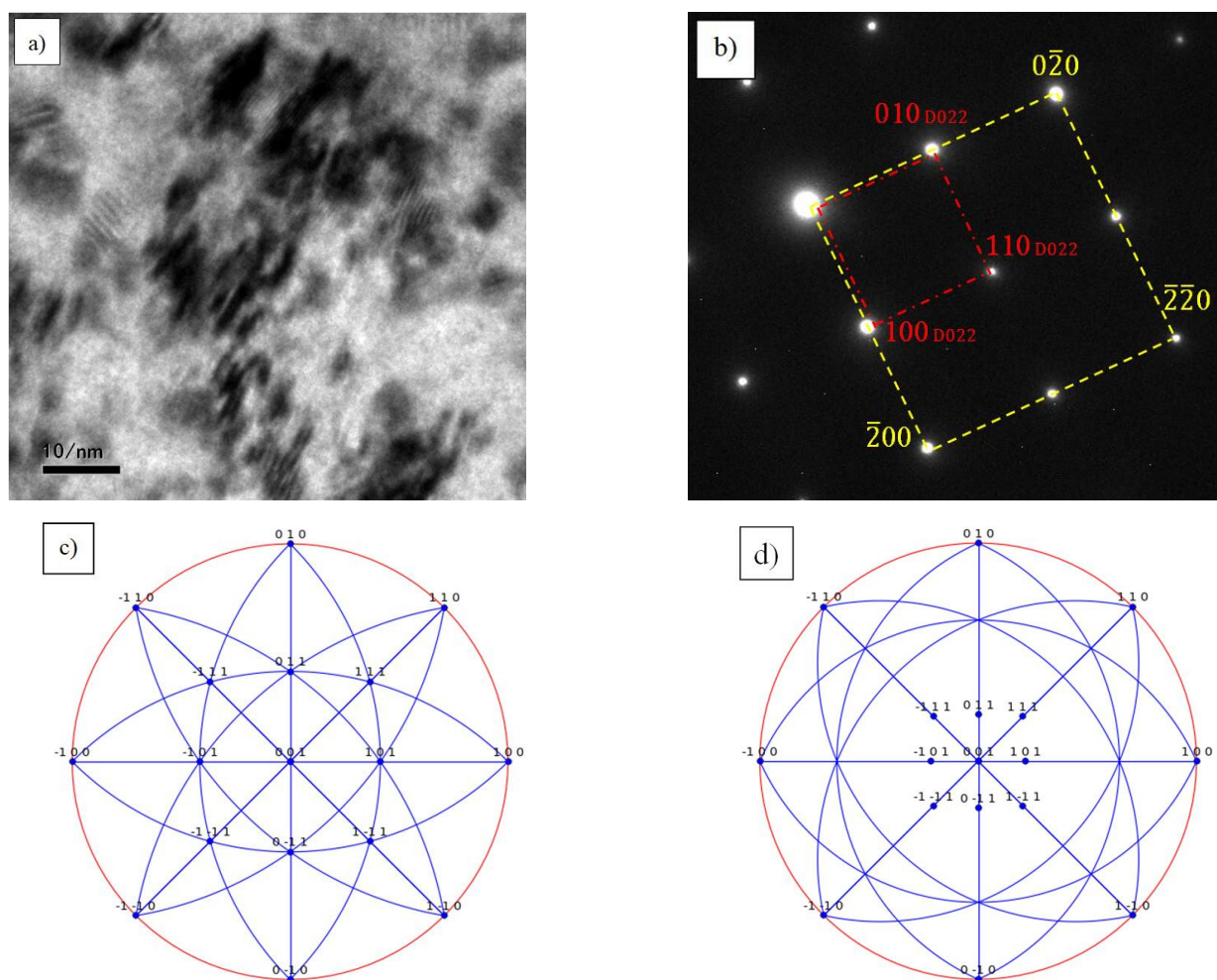


Figure 13. The TEM structure of $D0_{22}$ - Al_3Ta phase. (a) the morphology of $D0_{22}$ - Al_3Ta phase; (b) the diffraction pattern of $D0_{22}$ - Al_3Ta phase; (c) the stereographic projection of the matrix; (d) the stereographic projection of $D0_{22}$ - Al_3Ta phase.

4. Conclusions

Overall, first principles calculations have been performed on elastic anisotropy, electronic structures, and work function of $D0_{22}$ -type Al_3TM ($TM = Sc, Ti, V, Y, Zr, Nb, La, Hf, Ta$), including $Al_3Sc, Al_3Ti, Al_3V, Al_3Y, Al_3Zr, Al_3Nb, Al_3La, Al_3Hf$, and Al_3Ta , respectively. The obtained results agree with the existing theoretical values.

It is noted that the thermodynamic properties of the nine $D0_{22}$ -type compounds are stable. The alloying ability of the nine $D0_{22}$ -type compounds from strong to weak can be arranged as $Al_3Zr > Al_3Nb > Al_3Hf > Al_3Ti > Al_3Sc > Al_3Ta > Al_3Y > Al_3V > Al_3La$. The order of the bulk modulus of these $D0_{22}$ -type compounds is $Al_3Ta > Al_3Nb > Al_3V > Al_3Hf$

$> \text{Al}_3\text{Ti} > \text{Al}_3\text{Zr} > \text{Al}_3\text{Sc} > \text{Al}_3\text{Y} > \text{Al}_3\text{La}$. Specifically, Al_3Ta and Al_3La have the largest shear modulus (108.19 GPa) and smallest one (22.41 GPa) separately. It can be found that Al_3Ta and Al_3La have the largest Young's modulus (254.17 GPa) and smallest one (59.62 GPa). It is evident that Al_3Ta has the higher hardness and is not easy to deform.

Furthermore, the universal anisotropy of these D0_{22} -type compounds can be listed as $\text{Al}_3\text{La} > \text{Al}_3\text{Zr} > \text{Al}_3\text{Hf} > \text{Al}_3\text{Ti} > \text{Al}_3\text{Y} > \text{Al}_3\text{Sc} > \text{Al}_3\text{V} > \text{Al}_3\text{Nb} > \text{Al}_3\text{Ta}$. The Al_3La and Al_3Ta have the highest and lowest A_C values, demonstrating that the shear modulus anisotropy of Al_3La is the strongest, while that of Al_3Ta is the weakest. The A_3 value of Al_3La has the most deviation from 1, indicating that the Al_3La shows the highest shear anisotropy in the (001) plane. Except for Al_3Sc and Al_3La , the Young's modulus of other compounds in [001] direction is greater than that in [100] and [010] directions. From the standpoint of anisotropy, it is speculated that D0_{22} -type Al_3La may not exist.

It can be suggested that the density of states at Fermi level is not zero, suggesting that these phases have metal properties and electrical conductivity. Obviously, the pseudogap of Al_3Ta has the widest width, meaning that the covalent bond strength of Al_3Ta is stronger than that of Al_3V and Al_3Nb . The electron concentration between the Al and TM (V, Nb and Ta) atoms in Al_3V , Al_3Nb and Al_3Ta compounds is higher, which shows that Al-TM (V, Nb and Ta) bonds are stronger. Ultimately, the work function of Al_3La is the smallest on (100), demonstrating that the Young's modulus and Vickers hardness of Al_3La are the lowest.

Based on the calculated results, a kind of D0_{22} reinforced alloy was designed, which proves that this phase has an excellent strengthening effect. The matrix is strengthened by D0_{22} -type Al_3Ta phase, resulting in its tensile strength up to 1120 MPa and elongation up to 26%. The crystallographic relationship between D0_{22} -type Al_3Ta phase and matrix is $[001]_{\text{D0}_{22}} // [001]_{\text{Matrix}}$. The experimental results of this work further verify the reliability of the calculated results, which has important reference values for the design and application of the materials.

Author Contributions: Conceptualization, G.Z.; data curation, X.R.; formal analysis, F.S. and M.W.; funding acquisition, H.X.; investigation, H.L. and X.R.; methodology, H.L. and Y.F.; project administration, H.X.; resources, M.W.; software, Y.F.; supervision, G.Z.; validation, G.Z. and F.S.; writing—original draft, F.S.; writing—review & editing, H.L. All authors have read and agreed to the published version of the manuscript.

Funding: The present study was financially supported by the Fundamental Research Funds of China (237099000000170009), the Natural Science Foundation of Shanxi Province (201801D121108), the Key Research and Development (R&D) Projects of Shanxi Province (201803D121028).

Institutional Review Board Statement: Not applicable.

Informed Consent Statement: Not applicable.

Data Availability Statement: The data that support the findings of this study are available from the corresponding author upon reasonable request.

Conflicts of Interest: The authors declare no conflict of interest.

References

- Schön, C.G.; Duong, T.; Wang, Y.; Arróyave, R. A proof of concept: Thermodynamics of aluminum–transition metal highly concentrated alloys. *J. Alloy. Compd.* **2019**, *781*, 595–605. [[CrossRef](#)]
- Engelbert, S.; Janka, O. RE_4TAl (RE = Y, Sm, Gd–Tm, Lu; T = Pd, Pt)—Synthesis and magnetism of new aluminum representatives with the Gd 4 RhIn type structure. *Intermetallics* **2018**, *96*, 84–89. [[CrossRef](#)]
- Zhang, X.; Dong, T.; Ma, H.; Li, D.; Ying, C.; Liu, C.; Wang, F. A first principles investigation on the influence of transition-metal elements on the structural, mechanical, and anisotropic properties of $\text{CaM}_2\text{Al}_{20}$ intermetallics. *J. Mol. Graph. Model.* **2020**, *96*, 107509. [[CrossRef](#)]
- Zhu, M.; Wu, P.; Li, Q.; Xu, B. Vacancy-induced brittle to ductile transition of W-M co-doped Al_3Ti (M = Si, Ge, Sn and Pb). *Sci. Rep.* **2017**, *7*, 13964. [[CrossRef](#)] [[PubMed](#)]
- Khenioui, Y.; Boulechfar, R.; Maazi, N.; Ghemid, S. FP-LAPW investigation of $\text{Al}_3(\text{Sc}_{1-x}\text{Ti}_x)$ alloys properties in L1_2 and D0_{22} structures. *Int. J. Mod. Phys. B* **2018**, *32*, 1850167. [[CrossRef](#)]

6. Colinet, C.; Pasturel, A. Ab initio calculation of the formation energies of L1₂, D0₂₂, D0₂₃ and one dimensional long period structures in TiAl₃ compound. *Intermetallics* **2002**, *10*, 751–764. [[CrossRef](#)]
7. Colinet, C.; Pasturel, A. Phase stability and electronic structure of the HfAl₃ compound. *Phys. Rev. B* **2001**, *64*, 205102. [[CrossRef](#)]
8. Kwon, O.J.; Kim, Y.C.; Kim, K.B.; Lee, Y.K.; Fleury, E. Formation of amorphous phase in the binary Cu–Zr alloy system. *Met. Mater. Int.* **2006**, *12*, 207–212. [[CrossRef](#)]
9. Duan, Y.; Sun, Y.; Peng, M.; Zhou, S. Stability, elastic properties and electronic structures of L1₂-ZrAl₃ and D0₂₂-ZrAl₃ up to 40GPa. *J. Phys. Chem. Solids* **2014**, *75*, 535–542. [[CrossRef](#)]
10. Fuller, C.B.; Seidman, D.N. Temporal evolution of the nanostructure of Al (Sc, Zr) alloys: Part II-coarsening of Al₃(Sc_{1-x}Zr_x) precipitates. *Acta Mater.* **2005**, *53*, 5415–5428. [[CrossRef](#)]
11. Moon, K.I.; Lee, S.H.; Kim, S.J. The effect of Cu and Zn on the phase stability of L1₂ Al₃Hf intermetallic compound synthesized by mechanical alloying. *Intermetallics* **2002**, *10*, 793–800. [[CrossRef](#)]
12. Reshak, A.H.; Charifi, Z.; Baaziz, H. Ab-initio calculation of structural, electronic, and optical characterizations of the intermetallic trialuminides ScAl₃ compound. *J. Solid State Chem.* **2010**, *183*, 1290–1296. [[CrossRef](#)]
13. Li, J.; Zhang, M.; Luo, X. Theoretical investigations on phase stability, elastic constants and electronic structures of D0₂₂- and L1₂-Al₃Ti under high pressure. *J. Alloy. Compd.* **2013**, *556*, 214–220. [[CrossRef](#)]
14. Jahnátek, M.; Krajčí, M.; Hafner, J. Response of fcc metals and L1₂ and D0₂₂ type trialuminides to uniaxial loading along [100] and [001]: ab initio DFT calculations. *Philos. Mag.* **2011**, *91*, 491–516. [[CrossRef](#)]
15. Zhou, S.; Peng, B.; Cao, Y.; Xu, Y.; Quan, G.; Ma, S.; Jiao, Z.; Luo, K. First-principles investigations on stability, elastic properties and electronic structures of L1₂-TiAl₃ and D0₂₂-TiAl₃ under pressure. *Phys. B Condens. Matter* **2019**, *571*, 118–129. [[CrossRef](#)]
16. Jahnátek, M.; Krajčí, M.; Hafner, J. Interatomic bonds and the tensile anisotropy of trialuminides in the elastic limit: A density functional study for Al₃(Sc, Ti, V, Cr). *Philos. Mag.* **2007**, *87*, 1769–1794. [[CrossRef](#)]
17. Boulechar, R.; Meradji, H.; Ghemid, S.; Drablia, S.; Bouhafs, B. First principle calculations of structural, electronic and thermodynamic properties of Al₃(Ti_xV_{1-x}) alloy in D0₂₂ and L1₂ structures. *Solid State Sci.* **2013**, *16*, 1–5. [[CrossRef](#)]
18. Krajčí, M.; Hafner, J. Covalent bonding and bandgap formation in intermetallic compounds: A case study for Al₃V. *J. Phys. Condens. Matter.* **2002**, *14*, 1865–1879. [[CrossRef](#)]
19. Jahnátek, M.; Krajčí, M.; Hafner, J. Interatomic bonding, elastic properties, and ideal strength of transition metal aluminides: A case study for Al₃(V,Ti). *Phys. Rev. B* **2005**, *71*, 024101. [[CrossRef](#)]
20. Schwarz, R.; Desch, P.; Srinivasan, S.; Nash, P. Synthesis and properties of trialuminides with ultra-fine microstructures. *Nanostruct. Mater.* **1992**, *1*, 37–42. [[CrossRef](#)]
21. Chen, Z.; Zhang, P.; Chen, D.; Wu, Y.; Wang, M.; Ma, N.; Wang, H. First-principles investigation of thermodynamic, elastic and electronic properties of Al₃V and Al₃Nb intermetallics under pressures. *J. Appl. Phys.* **2015**, *117*, 085904. [[CrossRef](#)]
22. Colinet, C.; Pasturel, A. Phase stability and electronic structure in ZrAl₃ compound. *J. Alloy. Compd.* **2001**, *319*, 154–161. [[CrossRef](#)]
23. Li, R.-Y.; Duan, Y.-H. Electronic structures and thermodynamic properties of HfAl₃ in L1₂, D0₂₂ and D0₂₃ structures. *Trans. Nonferrous Met. Soc. China* **2016**, *26*, 2404–2412. [[CrossRef](#)]
24. Boulechar, R.; Meradji, H.; Chouahda, Z.; Ghemid, S.; Drablia, S.; Khenata, R. FP-LAPW investigation of the structural, electronic and thermodynamic properties of Al₃Ta compound. *Int. J. Mod. Phys. B* **2014**, *29*, 1450244. [[CrossRef](#)]
25. Li, C.; Cheng, N.; Chen, Z.; Xie, Z.; Hui, L. Intermetallic Growth and Interfacial Properties of the Grain Refiners in Al Alloys. *Materials* **2018**, *11*, 636. [[CrossRef](#)] [[PubMed](#)]
26. Pan, Y.; Li, Y.; Zheng, Q. Influence of Ir concentration on the structure, elastic modulus and elastic anisotropy of Nb Ir based compounds from first-principles calculations. *J. Alloy. Compd.* **2019**, *789*, 860–866. [[CrossRef](#)]
27. Zhang, Z.; Liao, N.; Zhou, H.; Xue, W. Insight into silicon-carbon multilayer films as anode materials for lithium-ion batteries: A combined experimental and first principles study. *Acta Mater.* **2019**, *178*, 173–178. [[CrossRef](#)]
28. Pham, T.N.; Ohno, K.; Sahara, R.; Kuwahara, R.; Bhattacharyya, S.; Thi, N.P. Clear evidence for element partitioning effects in a Ti-6Al-4V alloy by the first-principles phase field method. *J. Phys. Condens. Matter.* **2020**, *32*, 264001. [[CrossRef](#)]
29. Perdew, J.P.; Burke, K.; Ernzerhof, M. Generalized gradient approximation made simple. *Phys. Rev. Lett.* **1996**, *77*, 3865. [[CrossRef](#)]
30. Fadila, B.; Ameri, M.; Bensaid, D.; Nouredine, M.; Ameri, I.; Mesbah, S.; Al-Douri, Y. Structural, magnetic, electronic and mechanical properties of full-Heusler alloys Co₂YAl (Y = Fe, Ti): First principles calculations with different exchange-correlation potentials. *J. Magn. Magn. Mater.* **2018**, *448*, 208–220. [[CrossRef](#)]
31. Lishi, M.; Yonghua, D.; Runyue, L. Structural, elastic and electronic properties of C14-type Al₂M (M = Mg, Ca, Sr and Ba) Laves phases. *Phys. B Condens. Matter* **2017**, *507*, 147–155. [[CrossRef](#)]
32. Sun, F.; Zhang, G.; Ren, X.; Wang, M.; Xu, H.; Fu, Y.; Tang, Y.; Li, D. First-principles studies on phase stability, anisotropic elastic and electronic properties of Al-La binary system intermetallic compounds. *Mater. Today Commun.* **2020**, *24*, 101101. [[CrossRef](#)]
33. Duan, Y.-H.; Wu, Z.-Y.; Huang, B.; Chen, S. Phase stability and anisotropic elastic properties of the Hf–Al intermetallics: A DFT calculation. *Comput. Mater. Sci.* **2015**, *110*, 10–19. [[CrossRef](#)]
34. Bilic, A.; Gale, J.D.; Gibson, M.A.; Wilson, N.; McGregor, K. Prediction of novel alloy phases of Al with Sc or Ta. *Sci. Rep.* **2015**, *5*, 9909. [[CrossRef](#)] [[PubMed](#)]
35. Wang, X.; Zhao, W.; Cheng, Z.; Dai, X.; Khenata, R. Electronic, magnetic, half-metallic and mechanical properties of a new quaternary Heusler compound ZrRhTiTi: Insights from first-principles studies. *Solid State Commun.* **2018**, *269*, 125–130. [[CrossRef](#)]

36. Zhao, J.-S.; Gao, Q.; Li, L.; Xie, H.-H.; Hu, X.-R.; Xu, C.-L.; Deng, J.-B. First-principles study of the structure, electronic, magnetic and elastic properties of half-Heusler compounds LiXGe (X = Ca, Sr and Ba). *Intermetallics* **2017**, *89*, 65–73. [[CrossRef](#)]
37. Chong, X.; Jiang, Y.; Feng, J. Exploring the intrinsic ductile metastable Fe-C compounds: Complex chemical bonds, anisotropic elasticity and variable thermal expansion. *J. Alloy. Compd.* **2018**, *745*, 196–211. [[CrossRef](#)]
38. Sun, F.; Zhang, G.; Liu, H.; Xu, H.; Fu, Y.; Li, D. Effect of transition-elements substitution on mechanical properties and electronic structures of B2-AlCu compounds. *Results Phys.* **2021**, *21*, 103765. [[CrossRef](#)]
39. Puigdollers, A.R.; Alonso, G.; Gamallo, P. First-principles study of structural, elastic and electronic properties of α -, β - and γ -graphyne. *Carbon* **2016**, *96*, 879–887. [[CrossRef](#)]
40. Qin, H.; Yan, B.-L.; Zhong, M.; Jiang, C.-L.; Liu, F.-S.; Tang, B.; Liu, Q.-J. First-principles study of structural, elastic, and electronic properties of triclinic TATB under different pressures. *Phys. B Condens. Matter* **2019**, *552*, 151–158. [[CrossRef](#)]
41. Zheng, Y.; Wang, F.; Ai, T.; Li, C. Structural, elastic and electronic properties of B2-type modified by ternary additions FeAl-based intermetallics: First-principles study. *J. Alloy. Compd.* **2017**, *710*, 581–588. [[CrossRef](#)]
42. Zhao, Q.; Li, J.; Fang, Q.; Feng, H. Effect of Al solute concentration on mechanical properties of Al_xFeCuCrNi high-entropy alloys: A first-principles study. *Phys. B Condens. Matter* **2019**, *566*, 30–37. [[CrossRef](#)]
43. Roknuzzaman, M.; Hadi, M.; Ali, M.; Hossain, M.; Jahan, N.; Uddin, M.; Alarco, J.; Ostrikov, K. First hafnium-based MAX phase in the 312 family, Hf₃AlC₂: A first-principles study. *J. Alloy. Compd.* **2017**, *727*, 616–626. [[CrossRef](#)]
44. Liu, Y.; Hu, W.-C.; Li, D.-J.; Li, K.; Jin, H.-L.; Xu, Y.-X.; Xu, C.-S.; Zeng, X.-Q. Mechanical, electronic and thermodynamic properties of C14-type AMg₂ (A = Ca, Sr and Ba) compounds from first principles calculations. *Comput. Mater. Sci.* **2015**, *97*, 75–85. [[CrossRef](#)]
45. Panda, K.B.; Chandran, K.S. First principles determination of elastic constants and chemical bonding of titanium boride (TiB) on the basis of density functional theory. *Acta Mater.* **2006**, *54*, 1641–1657. [[CrossRef](#)]
46. Nye, J.F. *Physical Properties of Crystals*; Oxford University Press: Oxford, UK, 1985.
47. Lu, H.; Huang, X.; Li, N. Understanding the bond-energy, hardness, and adhesive force from the phase diagram via the electron work function. *J. Appl. Phys.* **2014**, *116*, 173506. [[CrossRef](#)]
48. Dong, Y.; Lu, H.; Cui, J.; Yan, D.; Yin, F.; Li, D. Mechanical characteristics of FeAl₂O₄ and AlFe₂O₄ spinel phases in coatings—A study combining experimental evaluation and first-principles calculations. *Ceram. Int.* **2017**, *43*, 16094–16100. [[CrossRef](#)]
49. Lu, H.; Li, L.; Huang, X.; Li, D. An electron work function based mechanism for solid solution hardening. *J. Alloy. Compd.* **2018**, *737*, 323–329. [[CrossRef](#)]
50. Liu, S.; Lu, H.; Li, D. The relationship between the electron work function and friction behavior of passive alloys under different conditions. *Appl. Surf. Sci.* **2015**, *351*, 316–319. [[CrossRef](#)]